# Calcium-dependent regulation of cyclic photosynthetic electron transfer by a CAS, ANR1, and PGRL1 complex

Mia Terashima[a,1,2], Dimitris Petroutsos[a,1], Meike Hüdig[a], Irina Tolstygina[a], Kerstin Trompelt[a], Philipp Gäbelein[a], Christian Fufezan[a], Jörg Kudla[a], Stefan Weinl[a], Giovanni Finazzi[b,c,d,e], and Michael Hippler[a,3]

[a]Institute of Plant Biology and Biotechnology, University of Münster, 48143 Münster, Germany; [b]Centre National Recherche Scientifique, Unité Mixte Recherche 5168, Laboratoire Physiologie Cellulaire et Végétale, F-38054 Grenoble, France; [c]Commissariat à l'Energie Atomique et Energies Alternatives, l'Institut de Recherches en Technologies et Sciences pour le Vivant, F-38054 Grenoble, France; [d]Université Grenoble 1, F-38041 Grenoble, France; and [e]Institut National Recherche Agronomique, F-38054 Grenoble, France

Edited by Elisabeth Gantt, University of Maryland, College Park, MD, and approved August 31, 2012 (received for review April 27, 2012)

**Cyclic photosynthetic electron flow (CEF) is crucial to photosynthesis because it participates in the control of chloroplast energy and redox metabolism, and it is particularly induced under adverse environmental conditions. Here we report that down-regulation of the chloroplast localized $Ca^{2+}$ sensor (CAS) protein by an RNAi approach in *Chlamydomonas reinhardtii* results in strong inhibition of CEF under anoxia. Importantly, this inhibition is rescued by an increase in the extracellular $Ca^{2+}$ concentration, inferring that CEF is $Ca^{2+}$-dependent. Furthermore, we identified a protein, anaerobic response 1 (ANR1), that is also required for effective acclimation to anaerobiosis. Depletion of ANR1 by artificial microRNA expression mimics the CAS-depletion phenotype, and under anaerobic conditions the two proteins coexist within a large active photosystem I-cytochrome $b_6/f$ complex. Moreover, we provide evidence that CAS and ANR1 interact with each other as well as with PGR5-Like 1 (PGRL1) in vivo. Overall our data establish a $Ca^{2+}$-dependent regulation of CEF via the combined function of ANR1, CAS, and PGRL1, associated with each other in a multiprotein complex.**

algae | acclimation, environmental stress (or environment and stress) and energy transduction

Photosynthesis is fundamental for life. In oxygenic photosynthesis, light either drives ATP and NADPH synthesis via linear photosynthetic electron transfer (LEF) or solely ATP production via cyclic electron flow (CEF). CEF is crucial to photosynthesis because it facilitates reequilibration of the ATP and NADPH pools for proper carbon assimilation and limits overreduction of the photosystem I (PSI) acceptor side (1–3). During CEF, electrons are reinjected into the photosynthetic electron transport chain either at the plastoquinone pool or at the stromal side of the cytochrome $b_6/f$ complex. Recently, a PSI–light-harvesting (PSI-LHCI)–PSII-LHCII–cytochrome $b_6/f$ supercomplex, competent in CEF was isolated from *Chlamydomonas reinhardtii* (4). This complex additionally contains the ferredoxin-NADPH oxidoreductase (FNR) and the thylakoid protein PGR5-Like 1 (PGRL1). PGRL1 is a component of the CEF machinery in *Arabidopsis thaliana* and *C. reinhardtii* (5, 6). Although photosynthetic electron transfer has been studied in detail, the regulation of CEF remains unknown. The induction of CEF has been described as an acclimation response to adverse environmental conditions (1, 2, 7). Generally, biological systems acclimate to environmental stresses to reestablish cellular homeostasis. Intracellular $Ca^{2+}$ changes often mediate such acclimation responses, triggering downstream signal transduction and changes in gene expression (8). $Ca^{2+}$-binding proteins are required for $Ca^{2+}$ sensing (9), and there is emerging evidence that chloroplasts may contribute to cellular $Ca^{2+}$ signaling via the chloroplast-localized $Ca^{2+}$ sensor protein CAS. CAS function is crucial for stomatal regulation (10, 11) and chloroplast-mediated activation of immune signaling (12) in *A. thaliana*, as well as effective photo-acclimation in *C. reinhardtii* by controlling the expression of light harvesting complex stress-related protein 3 (LHCSR3) (13). This protein is crucial for qE, the energy-dependent component of nonphotochemical quenching (NPQ), which regulates thermal dissipation of excess absorbed light energy (14). NPQ and photosynthetic CEF are interrelated because CEF contributes to the pH-gradient across the thylakoid membrane, which is required for efficient qE (15).

Correspondingly, in this study we addressed whether regulation of qE and CEF in *C. reinhardtii* are both linked to CAS and calcium-dependent regulation. We focused on anaerobic conditions because CEF is strongly induced under such growth settings (16). Recent quantitative proteomics data identified the thylakoid membrane protein thylakoid-enriched fraction 7 (TEF7) (17) (Joint Genome Institute v4.0 Protein ID 188287, hereafter designated as ANR1), as induced under anaerobic growth conditions in *C. reinhardtii* (18). Because CEF is stimulated under these circumstances, we investigated whether ANR1 function is important for CEF and interrelated to CAS functionality.

## Results

**ANR1, CAS, and PGRL1 Are Associated Together in a PSI-Dependent Multiprotein Complex.** In the green alga *C. reinhardtii*, CEF is strongly induced under anaerobic growth conditions (16). It is known that in *C. reinhardtii*, PGRL1 is required for efficient CEF under anaerobic conditions (16) and iron deficiency (6), although the mechanism of this correlation is still unexplained. Additional proteins that are induced under anaerobic conditions and associate with PSI may represent novel candidates mediating this unsolved regulation of CEF. To test whether ANR1, which is induced in expression under anoxic settings (18), is such a candidate, we investigated the accumulation of ANR1 in a PSI-deficient mutant (19). Accumulation of ANR1 is diminished in the absence of PSI under anaerobic conditions (Fig. 1*A*). Accordingly, we investigated whether ANR1 associates with PSI by solubilizing thylakoid membranes from anaerobic *C. reinhardtii* cells and separating the protein complexes by sucrose density centrifugation (Fig. 1*B*). SDS/PAGE separation of a fractionated sucrose gradient (starting at the bottom) and immunoblot localization of ANR1 and PSI (PsaD) revealed comigration of the two proteins around the high sucrose density fraction 6 (out of total 20) (Fig.1*C*). As expected, the PsaD signal peaked around

Author contributions: J.K., S.W., G.F., and M. Hippler designed research; M.T., D.P., M. Hüdig, I.T., K.T., P.G., S.W., and G.F. performed research; M.T., D.P., M. Hüdig, I.T., K.T., P.G., C.F., J.K., S.W., G.F., and M. Hippler analyzed data; and M.T., D.P., J.K., G.F., and M. Hippler wrote the paper.

The authors declare no conflict of interest.

This article is a PNAS Direct Submission.

[1]M.T. and D.P. contributed equally to this work.

[2]Present address: Department of Plant Biology, Carnegie Institution for Science, Stanford, CA 94305.

[3]To whom correspondence should be addressed. E-mail: mhippler@uni-muenster.de.

This article contains supporting information online at www.pnas.org/lookup/suppl/doi:10.1073/pnas.1207118109/-/DCSupplemental.

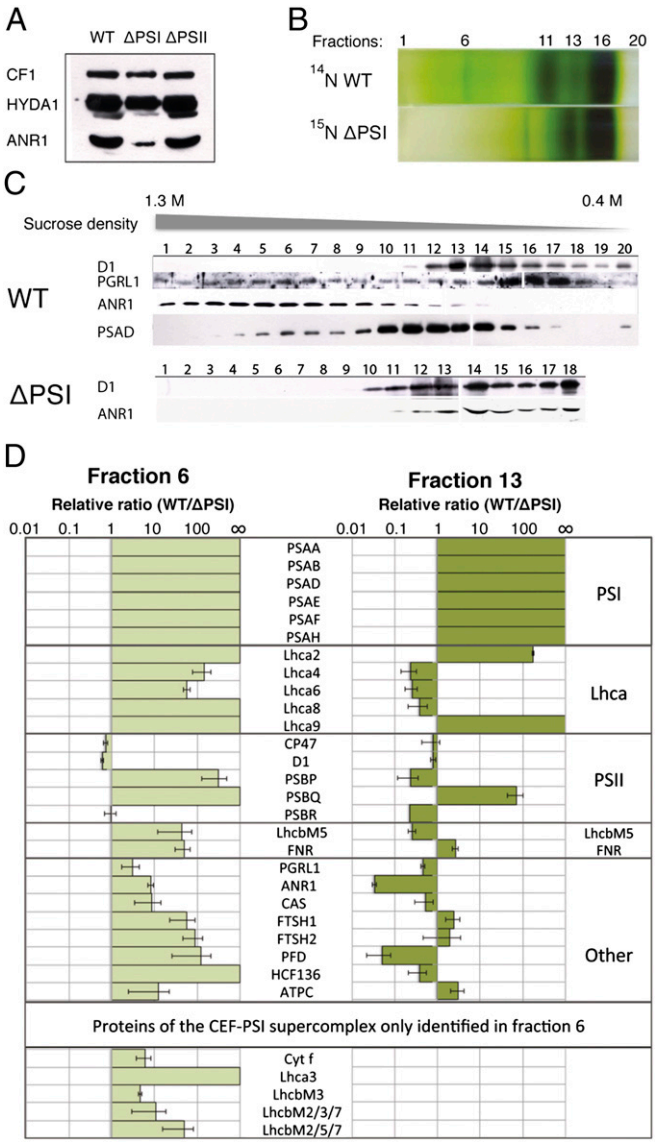


**Fig. 1.** ANR1 and CAS are components of the CEF supercomplex. (*A*) Immunoblot of anaerobic thylakoids isolated from WT, ΔPSI, and ΔPSII detects reduced levels of ANR1 in the ΔPSI strain. HYDA1 induction suggests anaerobic conditions. ATP synthase subunit CF1 is used as loading control. (*B*) SDG separation of WT and ΔPSI anaerobic thylakoids into 20 (F1–F20) fractions. (*C*) Immunoblot detection of ANR1 among the 20 fractions. ANR1 is localized to the higher-density region (F6) of the SDG in the WT, whereas in ΔPSI ANR1 is shifted to the lower-density region (F13). (*D*) WT SDG fractions 6 and 13 have been compared with the respective fractions from the $^{15}$N-labeled ΔPSI through quantitative MS. Equal volumes from each sample were mixed and analyzed to determine the relative protein ratios (WT/ΔPSI).

fraction 11, corresponding to the PSI-LHCI complex. Fraction 6 coincides with the location of the previously identified CEF supercomplex (4). Comigration of ANR1, PsaD, and PGRL1 in fraction 6 suggests that ANR1 may function as an additional subunit of the CEF supercomplex. Notably, ANR1 localization was shifted to the low-density region of the gradient in a ΔPSI strain, indicating that ANR1 migration is PSI-dependent (Fig. 1*C*). To identify interaction partners of ANR1 and therefore possible new components of the CEF supercomplex, we comparatively analyzed fractions 6 and 13 in WT and ΔPSI strains using quantitative mass spectrometry. Protein levels from $^{15}$N-labeled ΔPSI cells and WT cells were quantified with relative ratios represented as WT/ΔPSI. Among the 60 proteins identified in fraction 6 (supercomplex) and the 63 proteins quantified in fraction 13 (PSI), a total of 26 proteins were common to both fractions (Fig. 1*D*). Proteins of the PSI core complex (PSAA, PSAB, PSAD, PSAE, PSAF, and PSAH) were, as expected, only found in the unlabeled form, stemming from WT thylakoids (Fig. 1*D*). Photosystem I light-harvesting complex (LHCA) subunits were largely enriched in WT fraction 6, even though to a lesser extent compared with the core subunits. Lhca4, -6, and -8 were enriched in fraction 13 of ΔPSI because these subunits form a complex that accumulates independently of PSI at the thylakoid membrane, whereas Lhca2, -3, and -9 solely associate with PSI (20). LhcbM5, an LHCII protein, exhibits a similar distribution to Lhca4, -6, and -8, with higher abundance in fraction 6 for the WT and in fraction 13 for the ΔPSI, demonstrated by ratios of 43.4 (SD 31) and 0.256 (SD 0.049), respectively. These results are also in line with the accumulation of LhcbM5 in the PSI–LHCI–LHCII supercomplex (21). Subunits of PSII were also identified in the higher-density region of fraction 6. D1 was identified in addition to CP47 and the PSII extrinsic proteins PSBP, -Q, and -R (Fig. 1*D*). CP47 and D1 show comparable abundance between WT and ΔPSI in both fractions, whereas the extrinsic subunits PSBP, -Q, and -R were more variable.

Proteins exhibiting the same pattern as ANR1 of differential accumulation in WT and ΔPSI in fraction 6 and 13 are interesting because they represent additional possible components of the ANR1-containing supercomplex. Notably cyt*f* and PGRL1 were similarly enriched in fraction 6 as ANR1, strengthening the view that fraction 6 contains a CEF supercomplex potentially associated with ANR1. FNR, which is also part of the CEF supercomplex (4), exhibited a similar PSI dependence for localization to the higher-density region of the gradient. Its abundance in the high-density region is greatly reduced in the absence of PSI. Other proteins also displayed a change in their distribution between the high- and low-density region upon removal of PSI. This includes high chlorophyll fluorescence (HCF136), essential for PSII assembly (22), filamentation temperature-sensitive H 1 (FTSH1) and -2 metalloproteases, CAS, and a prefoldin-domain containing protein. In contrast, the ATP synthase γ chain (ATPγ) did not show a shift in distribution between the high- and low-density regions of the gradient.

Taken together, these data suggest that ANR1 could be part of the CEF supercomplex. Moreover, the calcium sensor CAS is identified as a possible component of the same complex. As outlined above, $Ca^{2+}$ is known to have crucial roles in signaling and regulating photo-acclimation in *C. reinhardtii* (13). Thus, CAS could potentially have a regulatory function in CEF. Neither CAS nor ANR1 were identified in the recently described CEF supercomplex (4).

**Spectroscopic Measurements Reveal Active Electron Transfer Between PSI and Cytochrome $b_6f$ Complex in Isolated CEF Supercomplex in Vitro.** To test whether our putative CEF supercomplex was functionally active we isolated the complex as described above (Fig. 1), but we refined the resolution of the sucrose density gradient by decreasing the fractionation volume (from 500 to 300 μL). Analyses of the resulting fractions (Fig. 2*A*) by SDS/PAGE and immunoblotting confirms comigration of CAS, ANR1, and PsaD in the region of the CEF supercomplex, peaking now at fraction 7 (Fig. 2*B*). Notably, as seen for ANR1 (Fig. 1*C*), CAS localization was shifted to the low-density region of the gradient in a ΔPSI strain, indicating that CAS migration is also PSI-dependent (Fig. S1). Spectroscopic measurements of the isolated CEF supercomplex reveal plastocyanin (PC)-dependent reduction and oxidation of cyt*b* and cyt*f*, as well as reduction of $P700^+$ (Fig. 2 *C* and *D*). After the light is switched on, the amplitudes of reduced cyt*b* and cyt*f* in the respective kinetic traces are significantly increased in the presence of 1 μM PC compared with the

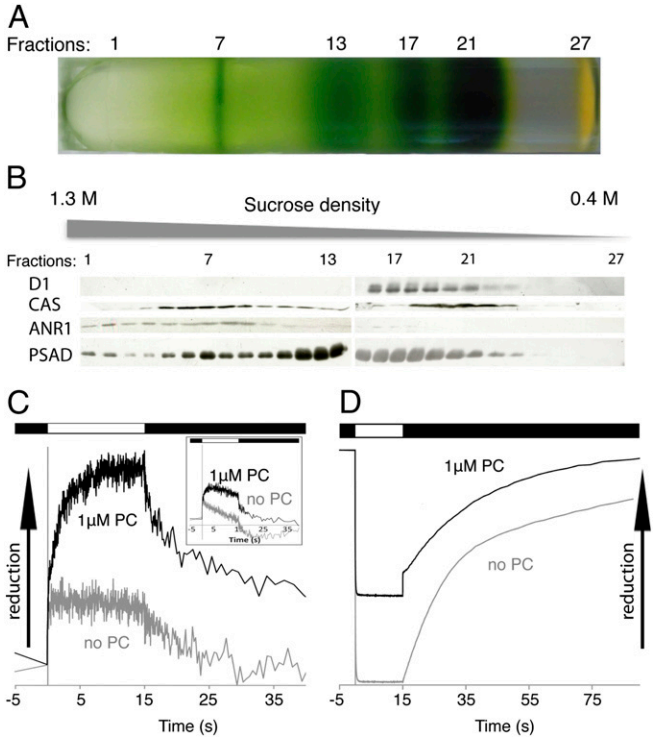


**Fig. 2.** Isolated CEF supercomplex shows PC-dependent electron transfer activity. (*A*) SDG separation of WT anaerobic thylakoids into 27 (F1–F27) fractions. (*B*) Immunoblot detection of ANR1 and CAS among the 27 TCA-precipitated fractions confirmed the localization of ANR1 and CAS to the higher-density region (peaking around F7) of the SDG in the WT. (*C*) Cytochrome *b* and cytochrome *f* (*Inset*) reduction (actinic light on) and oxidation (actinic light off) in the presence of 1 μM ferredoxin and absence and presence of 1 μM PC. Note that the electron transfer measurements were done in the presence of 200 μM methylviologen to avoid overaccumulation of reducing equivalent at the reducing side of PSI because ferredoxin mediates the rate-limiting step in CEF. (*D*) P700 oxidation and rereduction under continuous illumination followed by dark recovery, in the absence and presence of PC.

control without PC. After the light is turned off, oxidation kinetics for cyt*b* and cyt*f* in the presence of PC become biphasic, with a fast phase that is absent in the control lacking PC. This fast decay observed in the absorbance transients possess half-lives for cyt*b* and cyt*f* oxidation of 862 ms and 92 ms and amplitudes of 36% and 33% of the total signal, respectively. In the absence of PC, the resulting kinetic traces can be deconvoluted with one-exponential decay, yielding half-lives for cyt*b* and cyt*f* oxidation of 29 s and 1.4 s, respectively. Reduction of $P700^+$ after shifting from light to dark in the presence of 1 μM PC results in a biphasic kinetic trace that can be deconvoluted into a fast phase with a half-time of 9 ms and a slower ascorbate-dependent phase that is also observed in the control without PC. The half-time of 9 ms corresponds to a second-order electron transfer constant of electron transfer between PSI and PC of $7.7 \times 10^7\ M^{-1}\ s^{-1}$ a value that is expected for fast and functional electron transfer between PSI and PC (23). The decrease in amplitude of oxidized $P700^+$ in the presence of PC is due to the accelerated electron transfer between PC and PSI, so that less oxidized PSI can be spectroscopically detected in the given measurement time frame. Thus, these data confirm the presence of redox-active PSI and cytochrome $b_6/f$ complex in the CEF supercomplex fraction and indicate functionally active electron transfer between PSI and cytochrome $b_6/f$ complex. Thereby the spectroscopic data confirm the successful enrichment of an active CEF supercomplex via our isolation procedure.

**Bimolecular Fluorescence Complementation Verifies That CAS and ANR1 Interact with Each Other as Well as with PGRL1 in Vivo.** To further validate the protein–protein interaction of ANR1 and CAS as well as with the functional CEF-regulating protein PGRL1, we performed in vivo bimolecular fluorescence complementation (BiFC) heterologously by expressing the *C. reinhardtii* proteins in tobacco leaves. BiFC technology relies on the reconstitution of functional fluorescent complexes by two nonfluorescent fragments of the yellow fluorescent protein when putative interacting proteins fused to these fragments associate with each other (24, 25). To this end, the *C. reinhardtii* genes encoding *ANR1*, *CAS*, and *PGRL1* were codon-optimized and chemically synthesized for expression in vascular plants. Coding sequences of these genes were fused C-terminally either to $YFP^n$ or $YFP^c$ (24). Tobacco leaves infiltrated with Agrobacteria harboring $YFP^n$ and $YFP^c$ fusion constructs were analyzed by confocal laser scanning microscopy. BiFC-dependent fluorescence emission resulting from protein–protein interaction was exclusively observed in chloroplasts (Fig. 3). Consequently, these analyses reveal two important findings: (*i*) bimolecular fluorescence complementation and therefore direct protein–protein interactions between ANR1 and CAS, ANR1 and PGRL1, and CAS and PGRL1; and (*ii*) chloroplast localization of CAS, ANR1, and PGRL1. Remarkably, PGRL1, CAS, and ANR1 from *C. reinhardtii* also interacted with each of their *Arabidopsis* orthologs, suggesting that the protein–protein interaction motifs are conserved (Fig. S2).

**CEF Is $Ca^{2+}$ Regulated and Dependent on CAS and ANR1 Functions.** The observed CEF supercomplex colocalization as well as the BiFC-visualized protein–protein interaction between CAS, ANR1, and PGRL1 indicate that ANR1 and CAS are part of an active CEF supercomplex also including cytochrome $b_6/f$, PSI, and FNR. To further investigate the possible role of these proteins in CEF, artificial microRNA lines were generated. *Ami-RNA-anr1* strains show suppressed transcript levels as well as reduced protein levels compared with WT strains (Fig. S3 *A* and *B*). Spot tests to investigate growth under aerobic and anaerobic conditions on Tris–acetate–phosphate (TAP) medium and high-

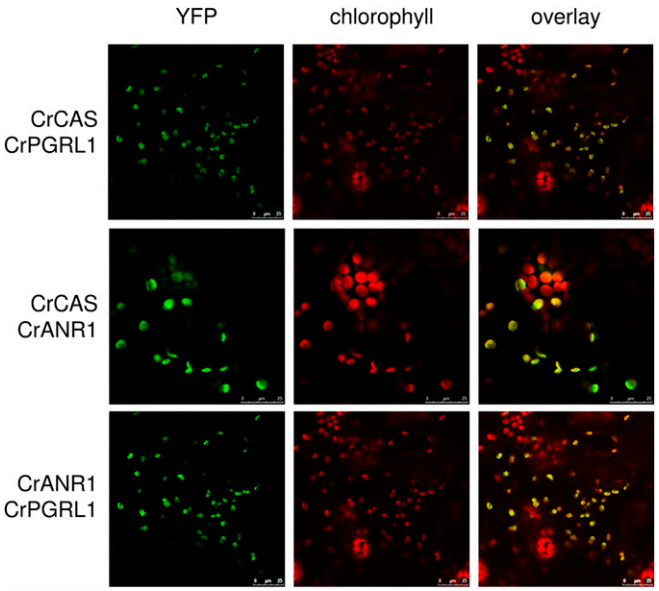


**Fig. 3.** *C. reinhardtii* CAS, ANR1, and PGRL1 interact with each other in vivo. BiFC interaction analysis of codon-optimized heterologously expressed *C. reinhardtii* proteins in *N. benthamiana* epidermal cells transiently expressing the plasmid combinations indicated at the left.

PLANT BIOLOGY

salt medium (HSM) under medium light revealed diminished growth for the artificial microRNA (*amiRNA*) strains under anaerobiosis (Fig. S3*C*), suggesting that lower protein levels of ANR1 result in compromised acclimation to anaerobic conditions. In line with this phenotype, *ami-RNA-anr1* strains showed delayed expression of a Fe-Fe-type hydrogenase (HYDA1), known to be induced under anoxic conditions (26, 27), after shift to oxygen deficiency (Fig. S4*A*). Quantitative proteomics revealed also an attenuated anaerobic response, demonstrated from the down-regulation of many proteins, including those usually induced under anoxia in the wild-type (18) (Fig. S4*B*).

To study the function of CAS, an RNAi strain with a twofold reduction in CAS protein level was chosen. This strain displayed an high light (HL)-sensitive phenotype that was rescued by the addition of a 10-fold higher $Ca^{2+}$ concentration, as previously described (13) (Fig. S5). CEF activity was investigated using WT, *pgrl1* knockout, and *ami-RNA-anr1-1*, as well as *ami-RNA-anr1-3* and *RNAi-cas-205* cells acclimated to $Ca^{2+}$-free medium and in the presence of 0.34 and 3.06 mM $Ca^{2+}$, respectively. LEF and CEF were measured spectroscopically with aerobic and anaerobic samples. Electron transfer rates were expressed as the relative amount of CEF (i.e., the fraction of electron flow through PSI that was insensitive to inhibition of PSII with 3-(3,4-dichlorophenyl)-1,1-dimethylurea (DCMU); Fig. 4) or as electrons per PSI per second (Fig. S6). Under aerobic conditions, no significant differences were observed. However, under anaerobic conditions in $Ca^{2+}$-free medium or at a $Ca^{2+}$ concentration of 0.34 mM, the CEF activity is approximately fourfold diminished in *ami-RNA-anr1-1* and *RNAi-cas-205* cells. In accordance with published data (16), CEF activity is also twofold lower in *pgrl1* and remains unaffected by $Ca^{2+}$. In contrast, CEF activity in *ami-RNA-anr1-1* and *RNAi-cas-205* cells is partially restored by increasing the extracellular $Ca^{2+}$ concentration to 3.06 mM. These data demonstrate that down-regulation of either ANR1 or CAS has a strong impact on CEF in a $Ca^{2+}$-dependent manner. In a related but independent experiment, we observed that down-regulation of CAS also impacts CEF under iron deficiency, as described for PGRL1-depletion mutants (6) (Fig. S7). Because CEF in the *ami-RNA-anr1* knockdown strains could not be rescued by an elevated $Ca^{2+}$ concentration to the same extent as observed for *RNAi-cas-205* cells, we asked whether the formation of the CEF supercomplex was impaired in these lines. This was not the case: mass spectrometric comparative quantitation of ΔPSI low-density sucrose fraction and *ami-RNA-anr1-1* CEF supercomplex revealed similar composition in the complex isolated from the *amiRNA* strain compared with WT (Fig. S8). Notably, we found that PGRL1 and CAS proteins were enriched in *ami-RNA-anr1-1* CEF supercomplex compared with the WT CEF supercomplex (Fig. S8), thus underpinning the association of CAS and PGRL1 with CEF supercomplex and possibly revealing a strategy to compensate for the lack of ANR1 in this complex.

## Discussion

In this study we investigated the role of ANR1 and CAS proteins in CEF using the green alga *C. reinhardtii*. First, our data identify ANR1 and CAS as crucial components of the CEF machinery, which was previously identified under state II conditions (4). Because neither PGRL1 nor ANR1 nor CAS are involved in state transitions (Fig. S9), the finding that CEF can be down-regulated by decreasing the cellular content of these proteins indicates that the link between CEF and state transitions (i.e., switch from LEF to CEF and state I to state II) is mostly phenomenological and not the same physical event. As suggested by the strong effect on CEF due to down-regulation of ANR1 and CAS (e.g., by far stronger than observed in *pgrl1*), these components of the CEF supercomplex seem to have a more prominent role than PGRL1 in this process.

Next, we reveal that cellular $Ca^{2+}$ homeostasis provides a fine-tuning modulation of CEF under anaerobic conditions in a CAS- and (to a less extent) ANR1-dependent manner. Loss of CAS function has been reported to impair stimulus-induced changes in cytoplasmic $Ca^{2+}$ dynamics (10), and we report here that CEF activity of the *ami-RNA-anr1* and *RNAi-cas-205* lines can also be restored by elevated $Ca^{2+}$ concentrations, although to a different degree. In particular, we propose that the calcium-binding protein CAS (28) could be directly involved in transducing changes in $Ca^{2+}$ concentration in the cytosol into chloroplast $Ca^{2+}$ responses (29), leading to changes in CEF activity by a still unknown mechanism. Indeed, elevation of external $Ca^{2+}$ totally restores CEF in *RNAi-cas* lines, and CAS- and $Ca^{2+}$-dependent regulation of CEF coincides with the regulation of LHCSR3 expression. Previously it has been reported that $Ca^{2+}$ uptake into the chloroplast occurs in the light, whereas $Ca^{2+}$ is released into the cytosol in the dark (30, 31). Accordingly, increased $Ca^{2+}$ concentration in the chloroplast in the light would facilitate induction of LHCSR3 expression and CEF via CAS and $Ca^{2+}$, which in turn strengthens qE and photo-protection of the alga. Nomura et al. (12) associated CAS with $^1O_2$-mediated retrograde signaling in *A. thaliana*, and taking these and the results presented here together, CEF could turn out to have a Janus-

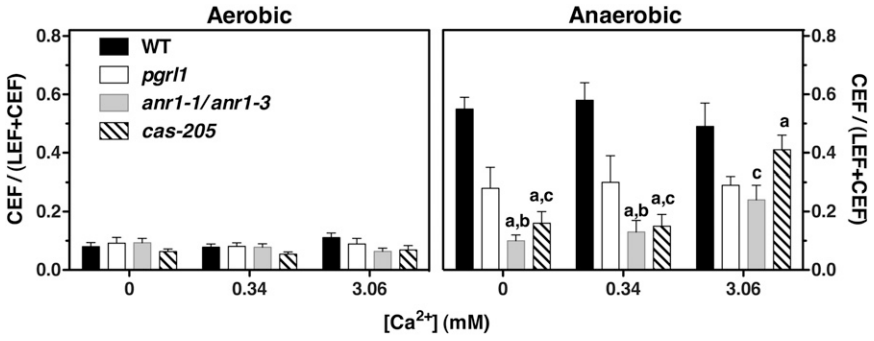


**Fig. 4.** Down-regulation of ANR1 or CAS results in diminished CEF, which is partially restored by increasing the extracellular $Ca^{2+}$ concentration. Relative amount of CEF under aerobic and anaerobic conditions in WT (21gr and *cw15-arg7*), *pgrl1*, *ami-RNA-anr1-1*, *ami-RNA-anr1-3*, and *RNAi-cas-205* grown in photoheterotrophic medium containing the indicated $Ca^{2+}$ concentrations. Data (±SD) refer to five measurements from three biological replicates for WT and *pgrl1* (10 and 13 measurements from five and seven biological replicates for *cas-205* and *anr1-1/anr1-3*, respectively). Statistical comparison was performed for the anaerobic data using one-way ANOVA followed by the Tukey multiple comparison test ($P < 0.01$). WT and *pgrl1* data were not affected by $Ca^{2+}$ concentration. Data for all mutants were significantly different from WT at all $Ca^{2+}$ concentrations, with the exception of *cas-205* at 3.06 mM $Ca^{2+}$. Lowercase letters in the graph denote significant differences: a, from *pgrl1*; b, from *anr1-1/anr1-3* at 3.06 mM $Ca^{2+}$; c, from *cas-205* at 3.06 mM $Ca^{2+}$. Comparison of all column pairs is given in Table S1.

faced function. On one hand, CEF is classically associated with ATP production without the production of NADPH; on the other hand, CEF leads to the reduction of the plastoquinone pool, thereby increasing the frequency of charge recombination events in PSII and as a result increasing $^1O_2$ production (32, 33). Thus, CAS and $Ca^{2+}$ via CEF could activate $^1O_2$-mediated retrograde signaling. Likewise, activation of CEF via CAS and $Ca^{2+}$ as observed in *C. reinhardtii* is in line with the inhibitory role of CAS in photosynthesis-driven $CO_2$ fixation, as suggested by Nomura et al. (12).

ANR1 likely plays a different role than CAS. Beside CEF, also NPQ is not restored in *ami-RNA-anr1-1* by elevated $Ca^{2+}$ (Fig. S10*A*), whereas a strong restoration of NPQ has been reported for *amiRNA-cas* lines after a 10-fold increase of external $Ca^{2+}$ in the growth medium (13). Moreover, treatment of ANR1 knockdown lines with a light intensity of 250 μE $m^{-2}$ $s^{-1}$ results in photosensitivity (Fig. S10*C*). In line with the reduced fitness observed in the *anr1* mutant in anoxia as well as high light, we propose that ANR1 could function as a molecular switch modulating the activity of the CEF supercomplex under harsh environmental conditions, like anoxia and high light, thereby enhancing fitness under oxygen deprivation or conditions of excess light. Indeed, formation of the CEF supercomplex is not inhibited in *ami-RNA-anr1-1* (Fig. S8), although its activity is drastically reduced (Fig. 4).

Consistent with this possibility, whereas CAS is conserved in algae and vascular plants, ANR1 represents an algae-specific protein, induced under anaerobic conditions and involved in the anaerobic responses (see phylogenetic tree, Fig. S11). Besides hydrogen production through HYDA1, fermentation pathways, usually known in prokaryotes, characterize the anaerobic metabolism of *C. reinhardtii* (34–36). Consequently, this alga seems to be well equipped for anoxic growth, a situation probably often encountered by this organism that is frequently found in eutrophic shallow ponds, rich in biomass and therefore subjected to periods of anoxia (37). Anaerobic conditions create a reducing environment in the chloroplast, leading to a limitation at the PSI acceptor side. Induction of HYDA1 and activation of CEF represent strategies to overcome this limitation. Whereas HYDA1 uses electrons to form hydrogen, CEF cycles electrons around the PSI and Cyt $b_6f$ complexes and produces ATP. The formation of the PSI-Cyt $b_6f$ supercomplex provides the molecular basis for this major energetic switch. By thermodynamically segregating the electron flow carriers capable of CEF within the chloroplast thylakoids, this complex may allow cells to maintain a high quantum yield of ATP synthesis to fuel various metabolic pathways. Similar requirements could be envisioned under excess light conditions, whereby a reducing environment in the chloroplast is equally established.

## Materials and Methods

**Strains and Growth Conditions.** The *C. reinhardtii* strains 21gr and cw15-arg7 (arginine-auxotroph) were used as WT controls of RNAi-cas and ami-RNA-anr1 mutant lines, respectively. The ΔPSI strain Δpsab and ΔPSII strain naq2 served as strains lacking PSI or PSII, respectively. The pgrl1 mutant (16) was used as a reference strain with impaired CEF. All strains were grown in standard TAP media at 25 °C under 20–50 μE $m^{-2}$ $s^{-1}$ light intensity. For quantitative mass spectrometric analyses, strains were handled as previously described (13). (*i*) Anaerobic induction: cells were grown to a density of 3–4 × $10^6$ cells $mL^{-1}$, and anaerobic conditions were induced by argon bubbling. The cultures were bubbled 4 h for immunoblot sampling and sucrose density gradients and 8 h for mass spectrometric comparison between ami-RNA-anr1-1 and WT. (*ii*) Cultures for spectroscopic measurements: WT and mutant cells, grown for 14 h in TAP medium containing 0, 0.34, and 3.06 mM $Ca^{2+}$ (standard TAP medium contains 0.34 mM $Ca^{2+}$) were harvested, pelleted, and resuspended in HSM (containing 0, 0.34, or 3.06 mM $Ca^{2+}$) at a cell density of 2 × $10^7$ cells $mL^{-1}$. The aerobic samples were shaken in the dark for at least 1 h before measurements. To induce anaerobiosis, cells were bubbled with nitrogen or argon for 2 h. (*iii*) High light response: cells grown in TAP under 20 μE $m^{-2}$ $s^{-1}$ were set at 2.5 μg chlorophyll $mL^{-1}$ and shifted for 4 h to 200 μE $m^{-2}$ $s^{-1}$ and HSM (no carbon source) containing 0.34 or 3.06 mM $Ca^{2+}$.

**Anaerobic Induction.** Cells were grown to a density of 3–4 × $10^6$ cells $mL^{-1}$, and anaerobic conditions were induced by argon bubbling. The cultures were bubbled for 4 h for immunoblot sampling and sucrose density gradients and for 8 h for mass spectrometric comparison between *ami-RNA-anr1-1*and WT.

**Generation of Artificial MicroRNA and RNAi Mutants.** Plasmid construction and generation of RNAi and amiRNA lines was done as described previously (13). Details are provided in *SI Materials and Methods*.

**Spot Test.** Cells were grown under standard conditions to early exponential growth phase and diluted to 1 × $10^6$ cells $mL^{-1}$. Ten microliters of the cells were spotted on TAP or HSM plates. Anaerobic bags (GENbag anaer from bioMériuex, REF 45 534) were used to create an anaerobic environment. Plates were incubated under 50 or 250 μE $m^{-2}$ $s^{-1}$ light.

**RT-PCR.** RT-PCR analysis of ami-RNA *tef7* was performed as previously described (18), with the primers listed in *SI Materials and Methods*.

**Immunoblots.** Protein analysis and immunodetection were performed as previously described (38, 39). Antibodies against ANR1 (against peptide sequence EEIYIGFVKEEGFGS) and against CAS (against peptide sequence ARADELDSTVESVVG) were purchased from Eurogentec. HYDA1 was a kind gift from Peter J. Nixon (Imperial College, London, United Kingdom). Proteins from fractions of sucrose density gradients (SDGs) were precipitated by addition of trichloroacetic acid to a final volume of 20% (vol/vol) and kept 2 h on ice, followed by an additional washing step with 100% (vol/vol) acetone. Pellets were resuspended in 50 mM $NH_4HCO_3$/8 M Urea and incubated for 15 min at room temperature before SDS/PAGE.

**Chloroplast and Thylakoid Isolation.** Chloroplasts were isolated as described by Naumann et al. (39), and thylakoids were isolated as previously described (6, 23).

**Mass Spectrometry.** Mass spectrometric analyses were performed as previously described (18). Details are provided in *SI Materials and Methods*.

**Sucrose Density Gradients.** Separation of photosynthetic protein complexes by a 1.3 M to 0.4 M SDG ultracentrifugation was done as described previously (21).

**Chlorophyll Fluorescence.** Cells grown in TAP under 20 μE $m^{-2}$ $s^{-1}$ were set at 2.5 μg chlorophyll $mL^{-1}$ and shifted for 4 h to 200 μE $m^{-2}$ $s^{-1}$ and HSM (no carbon source) containing 0.34 or 3.06 mM $CaCl_2$. Fluorescence was measured using a Maxi-Imaging PAM chlorophyll fluorometer (Heinz Walz). Samples were dark adapted for 20 min before each measurement. The effective photochemical quantum yield of photosystem II was measured as PSII yield [Y(II) = $(F_m'-F)/F_m'$)], whereas total NPQ was calculated as $(F_m - F'_m)/F_m'$. The variable fluorescence $F_v$ was calculated as $F_v = F_m - F_o$, and $F_v/F_m$ was used to evaluate the maximum fluorescence in the dark-adapted state; $F_m'$ is the maximum fluorescence in any light-adapted state; $F_o$ is the minimal fluorescence in the dark-adapted state.

**Spectroscopic Measurements.** WT and mutant cells, grown for 14 h in TAP medium containing 0, 0.34, and 3.06 mM $Ca^{2+}$ (standard TAP medium contains 0.34 mM $Ca^{2+}$) were harvested, pelleted, and resuspended in HSM (containing the appropriate $Ca^{2+}$ concentration) at a cell density of 2 × $10^7$ cells $mL^{-1}$. The aerobic samples were shaken in the dark for at least 1 h before measurements. To induce anaerobiosis, cells were bubbled with nitrogen or argon for 2 h.

LEF and CEF were measured by following the relaxation kinetics of the carotenoid electrochromic bandshift at 520 nm (corrected with the bandshift at 546 nm) in the absence and presence of 10 μM DCMU, respectively. Results were expressed as $e^{-1}$ $s^{-1}$ $PSI^{-1}$ upon normalization to the PSI amount. The latter was estimated from the amplitude of the electrochromic shift signal upon excitation with a saturating single turnover flash (5 ns laser pulse) in the presence of 10 μM DCMU and 1 mM hydroxylamine, to fully block PSII photochemistry.

For the CEF supercomplex activity, all measurements were performed using isolated CEF supercomplex at 20 μg Chl $mL^{-1}$ after addition of 200 μM methyl-viologen, 1 μM ferredoxin, 1 mM ascorbate, 2 mM $MgCl_2$, and 0.05% dodecyl-beta-D-maltoside. For measurements in the absence of PC samples were dark-adapted for 15 min. After addition of PC samples were dark-incubated at room temperature until the signal was stabilized. Cyt*f* redox changes were calculated as the difference between the absorption at 554 nm and a baseline drawn between 546 and 573 nm (40). Similarly, cyt*b* redox

changes were calculated as the difference between the absorption at 563 nm and a baseline drawn between 546 and 574 nm. Fitting of absorbance transients using one- and/or two-phase exponential decay was performed with GraphPad Prism version 5.01 for Windows (GraphPad Software).

**BiFC Analysis.** Coding sequences for Chlamydomonas *CAS*, *PGRL1*, and *ANR1* were codon-optimized for expression in plants, chemically synthesized, and cloned into pGPTV plant transformation vectors. Resulting constructs were transformed to *Nicotiana benthamiana* leaves by Agrobacterium-mediated transformation for heterologous expression and interaction analysis as previously described (41, 42).

**ACKNOWLEDGMENTS.** This work was supported by grants from the Deutsche Forschungsgemeinschaft (to J.K. and M. Hippler), the Seventh Framework Programme FP-7-SUNBIOPATH European Union project (to M. Hippler), and the Human Frontier Science Project (to J.K.), and by Grant PHYTADAPT 8NT09567009 from Agence Nationale de la Recherche (to G.F.).

1. Shikanai T (2007) Cyclic electron transport around photosystem I: Genetic approaches. *Annu Rev Plant Biol* 58:199–217.
2. Joliot P, Joliot A (2006) Cyclic electron flow in C3 plants. *Biochim Biophys Acta* 1757: 362–368.
3. Arnon DI (1959) Conversion of light into chemical energy in photosynthesis. *Nature* 184:10–21.
4. Iwai M, et al. (2010) Isolation of the elusive supercomplex that drives cyclic electron flow in photosynthesis. *Nature* 464:1210–1213.
5. DalCorso G, et al. (2008) A complex containing PGRL1 and PGR5 is involved in the switch between linear and cyclic electron flow in *Arabidopsis*. *Cell* 132:273–285.
6. Petroutsos D, et al. (2009) PGRL1 participates in iron-induced remodeling of the photosynthetic apparatus and in energy metabolism in *Chlamydomonas reinhardtii*. *J Biol Chem* 284:32770–32781.
7. Eberhard S, Finazzi G, Wollman FA (2008) The dynamics of photosynthesis. *Annu Rev Genet* 42:463–515.
8. Dodd AN, Kudla J, Sanders D (2010) The language of calcium signaling. *Annu Rev Plant Biol* 61:593–620.
9. Kudla J, Batistic O, Hashimoto K (2010) Calcium signals: The lead currency of plant information processing. *Plant Cell* 22:541–563.
10. Weinl S, et al. (2008) A plastid protein crucial for $Ca^{2+}$-regulated stomatal responses. *New Phytol* 179:675–686.
11. Nomura H, Komori T, Kobori M, Nakahira Y, Shiina T (2008) Evidence for chloroplast control of external $Ca^{2+}$-induced cytosolic $Ca^{2+}$ transients and stomatal closure. *Plant J* 53:988–998.
12. Nomura H, et al. (2012) Chloroplast-mediated activation of plant immune signalling in *Arabidopsis*. *Nat Commun* 3:926.
13. Petroutsos D, et al. (2011) The chloroplast calcium sensor CAS is required for photoacclimation in *Chlamydomonas reinhardtii*. *Plant Cell* 23:2950–2963.
14. Peers G, et al. (2009) An ancient light-harvesting protein is critical for the regulation of algal photosynthesis. *Nature* 462:518–521.
15. Busch A, Hippler M (2011) The structure and function of eukaryotic photosystem I. *Biochim Biophys Acta* 1807:864–877.
16. Tolleter D, et al. (2011) Control of hydrogen photoproduction by the proton gradient generated by cyclic electron flow in *Chlamydomonas reinhardtii*. *Plant Cell* 23: 2619–2630.
17. Allmer J, Naumann B, Markert C, Zhang M, Hippler M (2006) Mass spectrometric genomic data mining: Novel insights into bioenergetic pathways in *Chlamydomonas reinhardtii*. *Proteomics* 6:6207–6220.
18. Terashima M, Specht M, Naumann B, Hippler M (2010) Characterizing the anaerobic response of *Chlamydomonas reinhardtii* by quantitative proteomics. *Mol Cell Proteomics* 9:1514–1532.
19. Redding K, et al. (1998) A systematic survey of conserved histidines in the core subunits of Photosystem I by site-directed mutagenesis reveals the likely axial ligands of P700. *EMBO J* 17:50–60.
20. Takahashi Y, Yasui TA, Stauber EJ, Hippler M (2004) Comparison of the subunit compositions of the PSI-LHCI supercomplex and the LHCI in the green alga *Chlamydomonas reinhardtii*. *Biochemistry* 43:7816–7823.
21. Takahashi H, Iwai M, Takahashi Y, Minagawa J (2006) Identification of the mobile light-harvesting complex II polypeptides for state transitions in *Chlamydomonas reinhardtii*. *Proc Natl Acad Sci USA* 103:477–482.
22. Meurer J, Plücken H, Kowallik KV, Westhoff P (1998) A nuclear-encoded protein of prokaryotic origin is essential for the stability of photosystem II in *Arabidopsis thaliana*. *EMBO J* 17:5286–5297.
23. Hippler M, Drepper F, Farah J, Rochaix JD (1997) Fast electron transfer from cytochrome c6 and plastocyanin to photosystem I of *Chlamydomonas reinhardtii* requires PsaF. *Biochemistry* 36:6343–6349.
24. Hu CD, Chinenov Y, Kerppola TK (2002) Visualization of interactions among bZIP and Rel family proteins in living cells using bimolecular fluorescence complementation. *Mol Cell* 9:789–798.
25. Walter M, et al. (2004) Visualization of protein interactions in living plant cells using bimolecular fluorescence complementation. *Plant J* 40:428–438.
26. Stuart TS, Gaffron H (1972) The gas exchange of hydrogen-adapted algae as followed by mass spectrometry. *Plant Physiol* 50:136–140.
27. Happe T, Hemschemeier A, Winkler M, Kaminski A (2002) Hydrogenases in green algae: do they save the algae's life and solve our energy problems? *Trends Plant Sci* 7: 246–250.
28. Han S, Tang R, Anderson LK, Woerner TE, Pei ZM (2003) A cell surface receptor mediates extracellular $Ca^{(2+)}$ sensing in guard cells. *Nature* 425:196–200.
29. Stael S, et al. (2012) Cross-talk between calcium signalling and protein phosphorylation at the thylakoid. *J Exp Bot* 63:1725–1733.
30. Roh MH, Shingles R, Cleveland MJ, McCarty RE (1998) Direct measurement of calcium transport across chloroplast inner-envelope vesicles. *Plant Physiol* 118:1447–1454.
31. Kreimer G, Melkonian M, Holtum JAM, Latzko E (1985) Characterization of calcium fluxes across the envelope of intact spinach-chloroplasts. *Planta* 166:515–523.
32. Fufezan C, Rutherford AW, Krieger-Liszkay A (2002) Singlet oxygen production in herbicide-treated photosystem II. *FEBS Lett* 532:407–410.
33. Krieger-Liszkay A, Fufezan C, Trebst A (2008) Singlet oxygen production in photosystem II and related protection mechanism. *Photosynth Res* 98:551–564.
34. Hemschemeier A, Happe T (2005) The exceptional photofermentative hydrogen metabolism of the green alga *Chlamydomonas reinhardtii*. *Biochem Soc Trans* 33: 39–41.
35. Grossman AR, et al. (2007) Novel metabolism in *Chlamydomonas* through the lens of genomics. *Curr Opin Plant Biol* 10:190–198.
36. Terashima M, Specht M, Hippler M (2011) The chloroplast proteome: A survey from the *Chlamydomonas reinhardtii* perspective with a focus on distinctive features. *Curr Genet* 57:151–168.
37. Peers G, Niyogi KK (2008) Pond scum genomics: The genomes of *Chlamydomonas* and *Ostreococcus*. *Plant Cell* 20:502–507.
38. Hippler M, Klein J, Fink A, Allinger T, Hoerth P (2001) Towards functional proteomics of membrane protein complexes: Analysis of thylakoid membranes from *Chlamydomonas reinhardtii*. *Plant J* 28:595–606.
39. Naumann B, Stauber EJ, Busch A, Sommer F, Hippler M (2005) N-terminal processing of Lhca3 Is a key step in remodeling of the photosystem I-light-harvesting complex under iron deficiency in *Chlamydomonas reinhardtii*. *J Biol Chem* 280:20431–20441.
40. Finazzi G, et al. (1997) Function-directed mutagenesis of the cytochrome b6f complex in *Chlamydomonas reinhardtii*: Involvement of the cd loop of cytochrome b6 in quinol binding to the Q(o) site. *Biochemistry* 36:2867–2874.
41. Batistic O, Waadt R, Steinhorst L, Held K, Kudla J (2010) CBL-mediated targeting of CIPKs facilitates the decoding of calcium signals emanating from distinct cellular stores. *Plant J* 61:211–222.
42. Waadt R, et al. (2008) Multicolor bimolecular fluorescence complementation reveals simultaneous formation of alternative CBL/CIPK complexes in planta. *Plant J* 56: 505–516.